Quantifying present and projected future atmospheric moisture transports onto land

Matthias Zahn[1,2] and Richard P. Allan[3]

Received 31 October 2012; revised 4 September 2013; accepted 9 October 2013; published 6 November 2013.

[1] Changing properties of the landward moisture transports play a key role in assessing water availability in a warmed future world. Here the ocean-land moisture transports and their projected changes in a warmed atmosphere are investigated using high space and time resolution ECHAM5-model data representative for the current and future atmosphere. The water budgets are estimated from four-times daily instantaneous moisture transports across the shore-lines marking the boundaries of the land areas and from accumulated precipitation-evaporation over land. The transports are presented in very high detail with vertical profiles for each boundary segment. The results indicate land- and seaward moisture transports to intensify with warming. Generally, the landward transports increase stronger than the seaward transports resulting in increased moisture budgets too. This means a higher future average availability of water for land areas. Comparison of the budgets from moisture transports and precipitation-evaporation reveals a systematic bias. This has been linked to numerical issues in previous studies, but we here show that it is connected to the high variability over the diurnal cycle and the maxima of landward transports are likely not considered for many of the regions.

Citation: Zahn, M., and R. P. Allan (2013), Quantifying present and projected future atmospheric moisture transports onto land, *Water Resour. Res.*, *49*, 7266–7277, doi:10.1002/2012WR013209.

1. Introduction

[2] Replenishment of land water resources results almost entirely from precipitation, which itself depends on atmospheric moisture transports into a particular region. Over a sufficiently long time scale, all water available to human societies and terrestrial ecosystems originates from the ocean. Here it evaporates at the surface and is then shifted with atmospheric circulations until it precipitates back to the surface. Approximately 90% of this moisture is lost back to the ocean again, leaving the remaining 10% to be transported and precipitate onto the Earth's land areas [*Gimeno et al*., 2010a]. Thus, precipitation and water supply over land and their changes are crucially dependent on these moisture transports.

[3] Global warming and associated changes in atmospheric circulations and water holding capacities are expected to change various aspects of the hydrological cycle, amongst others the intensity of atmospheric water transports [*Zahn and Allan*, 2013]. Changes of the properties of such transports affect the future local water budgets and thus the local resources and availability of water. To prepare human societies for threats and benefits of such future changes, knowledge of this budget and of the transports and its changes is vital.

[4] A key response of the hydrological cycle in a warmed atmosphere is an increase of low-level atmospheric water vapor of 7% per degree of warming derived from theoretical considerations (Clausius-Clapeyron relation, e.g., *Wentz and Schabel* [2000]; *Trenberth et al*. [2003]; *Held and Soden* [2006]; *O'Gorman and Muller* [2010]). More atmospheric water vapor has a potentially strengthening impact on moisture transports and on precipitation.

[5] One of the first studies on oceanic source-continental sink relations and model-based moisture transports has been published by *Koster et al*. [1986]. They defined source and sink regions and estimated the water input in one sink as a percentage of the various source regions the water originates from. They found, that in the high and midlatitudes, water is more likely to originate from nearby sources and to be locally recycled, whereas in low latitude tropical regions, precipitation is more likely to stem from oceanic regions farther away. In a similar study, *Numaguti* [1999] shows source sink relations for Eurasia, finding the North Atlantic to be the source for its northern part, and the North Pacific only influencing the eastern edge of Asia.

[6] Recently applying reanalysis data from 1999 to 2008, *van der Ent et al*. [2010] investigated atmospheric precipitation from the point the water has last evaporated, which may have been from water or land covered surface. After being transported over land, water may precipitate and evaporate several times before being discharged back into the ocean again, a process denoted by the term recycling ratio and which is the main focus of their study. In the same year, *Gimeno et al*. [2010a] have published a study

Additional supporting information may be found in the online version of this article.

[1]Department of Meteorology, University of Reading, Reading, UK.
[2]Helmholtz-Zentrum Geesthacht, Geesthacht, Germany.
[3]Department of Meteorology, National Centre for Atmospheric Sciences, University of Reading, Reading, UK.

Corresponding author: M. Zahn, Helmholtz-Zentrum Geesthacht, Max-Planck-Strae 1, DE-21502 Geesthacht, Germany. (matthias.zahn@hzg.de)

0043-1397/13/10.1002/2012WR013209

applying a 3-D Lagrangian model [*Stohl and James*, 2004, 2005] to trace water particles from evaporation to precipitation globally, which enabled the quantification of detailed source-sink relations for atmospheric moisture. This model has also been used with reanalysis data for spatially more restricted regions, e.g., Central America [*Durán-Quesada et al*., 2010], Brazil [*Drumond et al*., 2008], India [*Ordóñez et al*., 2012], Spain [*Gimeno et al*., 2010b], Ethiopia [*Viste and Sorteberg*, 2011] or for the Sahel zone in north-western Africa [*Nieto et al*., 2006]. Also for the north-western African region *Hagos and Leung* [2012] have investigated the role latent and nonlatent heating play in moisture supply and at the eastern side of Africa, climate warming related changes of precipitation have been investigated, e.g., at basin scale for the Nyando River in Kenya [*Mutua et al*., 2012]. Moisture transports during wet events of the South America monsoon have been investigated by *Carvalho et al*. [2011]. On a very short term for individual extreme events, *Lavers et al*. [2011] demonstrate the importance of so called atmospheric rivers, narrow bands of enhanced moisture flux at 900 hPa, which were found to be responsible for flooding in parts of the United Kingdom.

[7] While these are nice studies on the source-sink relationships for moisture, they do not specifically provide any details on the continental moisture balance and their changes with warming. Such comprehensive moisture budgets for several continents are for example provided by *Trenberth et al*. [2007]. They estimate the budged based on reanalysis data for precipitation and evaporation over a period of 21 years in the past, 1979–2000, but do not provide estimates of any changes in a warmed future.

[8] We here investigate the budgets of each of the global land masses from an Eulerian perspective, in which the moisture budgets are determined by precipitation and evaporation data as well as by wind driven moisture transports over the coastal lines. The latter allow for investigations on where the moisture transports take place and where they may change. We deliberately do not discriminate between different climate regimes, but rather calculate moisture transports across the boundaries determined by the coastal lines. This enables us to calculate budgets for the continents valid for the current climate and compare with the *Trenberth et al*. [2007] data on the one hand-side, but applying IPCC future scenario [*Nakicenovic and Swart*, 2000] simulations on the other hand also enables us to assess any possible future changes individually for each continent.

[9] In this study, we specifically focus on the projected changes of ocean to land moisture transports. For a more complete overview on climate warming related changes of the hydrological cycle, the reader may be referred to studies of other authors, e.g., to the summary paper of *Gimeno et al*. [2012] or to *Seager et al*. [2010], who break down global warming related changes of the hydrological cycle into the dynamic and thermodynamic components and investigate their influences in different parts of the world, or to *Quante and Matthias* [2006], who describe the properties of water in the atmosphere in general.

2. Data and Method

[10] Moisture transports are estimated by linking water loads of atmospheric parcels with the wind vectors moving them through space. For computational reasons, this is often done using time mean values of these quantities; this is not physically consistent as mean wind vectors do not account for the direction of the actual instantaneous wind-vector at the time of a particular moisture load. Thus, if maxima/minima of wind and moisture content emerge simultaneously, using the mean wind would vastly underestimate the transports. Imagine, e.g., a Gaussian distribution of wind (positive and negative values denoting in- and outward transports) with a mean of zero would result in no moisture transport, although if in this case positive/negative wind speeds were associated with high/low moisture loads the total instantaneous sums would actually be positive as well.

[11] In our previous studies [*Zahn and Allan*, 2011, 2013] investigating past and anticipated warmed future changes of moisture transports into the tropical regions of convection, we have demonstrated the necessity of using instantaneous humidity scalars and instantaneous wind vectors to capture the coincidence of in- and outflow of moisture correctly. Thus, when studying a region's moisture budget it is important to have high space and time resolution data available.

[12] We here applied 6 hourly T213 (0.5°) horizontal resolution ECHAM5 model [*Roeckner et al*., 2003] data at 31 vertical levels representative for two time slices of 31 years, 1959–1989 (C20) and 2069–2099 (C21). The simulations are of the time slice type forced with boundary data (Sea Surface Temperature and Sea Ice) from a coupled climate simulation with the same model at T63 resolution. The C20 uses observed Greenhouse Gas and aerosol forcing, the C21 forcing was delivered by the A1B scenario [*Nakicenovic and Swart*, 2000] of the Fourth Assessment Report (AR4) of the Intergovernmental Panel of Climate Change (IPCC).

[13] To calculate the moisture transport (MT), we use the same formula from the same code as in our previous work, which estimates MT at time t along all the n_b boundary segments b and at all n_l vertical model levels l between grid boxes covered by ocean and those covered by land

$$\mathrm{MT}_t = \sum_b^{n_b} \sum_l^{n_l} \mathrm{WP}_{bl} \cdot \mathrm{PWC}_{bl} \tag{1}$$

[14] WP is the perpendicular wind vector (positive toward land) and PWC the precipitable water content. The calculations are performed on the model's $n_l = 31$ sigma levels. For each segment on each level, MT then is the product of WP and PWC. Note that this procedure results in a total of $n_b * n_l = 7810 * 31 = 242110$ segments across which individual transports are calculated. This is a special case of the divergence theorem in which the moisture flux is calculated along the boundaries of the continental shorelines.

[15] The lines marking the boundaries as derived from ECHAM5 are given in Figure1. Throughout this paper, we use acronyms for each land area as listed in Table 1. The areas cover the larger continents as well as several smaller islands. MT is calculated for each land area individually allowing intercomparisons. Continental waters such as the Baltic Sea or the Hudson Bay in Europe (EUR) and North America (NAM) are artificially treated as land grid boxes.

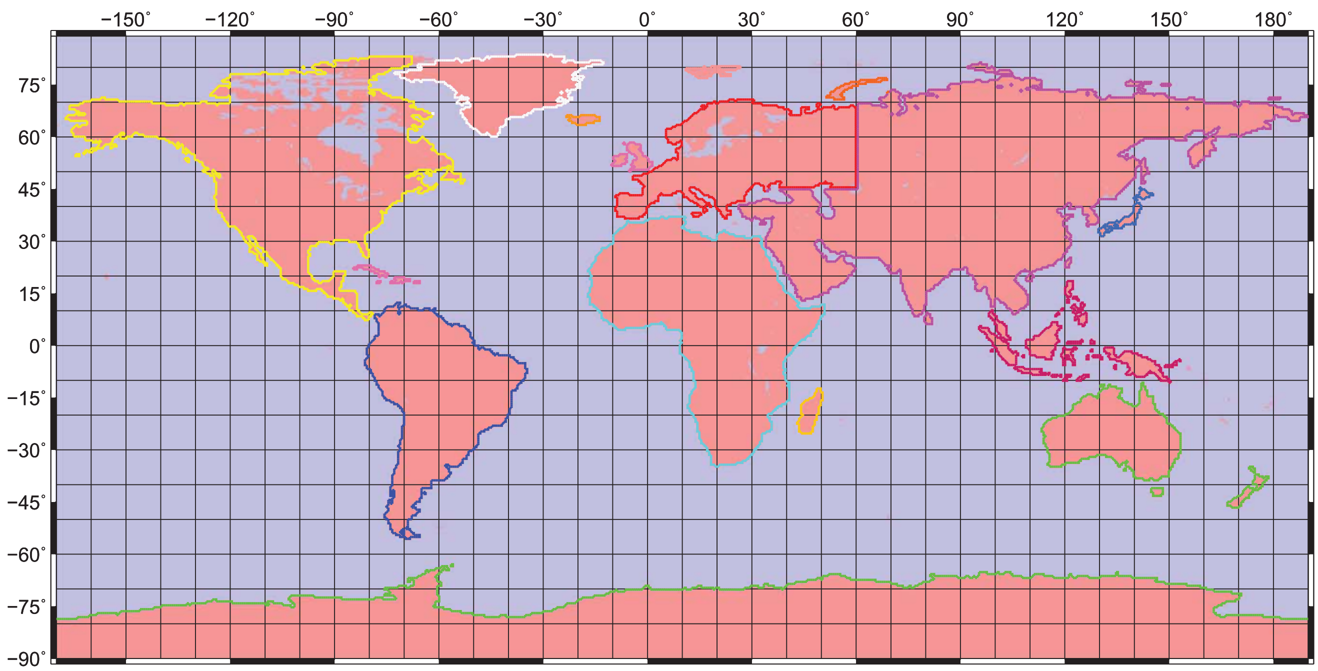

Figure 1. Continents and island and their boundaries. Land-sea mask from ECHAM5 and the boundaries across which the moisture transports have been calculated.

Although in an old study, [*Rasmusson*, 1971] water budgets of small areas were found to be less accurate than those of larger areas we here also include several smaller islands.

[16] The budgets of the calculated MTs will be compared with budgets derived from the precipitation evaporation balance, named PE. Assuming negligible changes in atmospheric moisture storage over the relatively short time period investigated, MT and PE should approximately compensate each other. In other words, we calculated the fluxes into atmospheric boxes bounded by imaginary walls built over the shorelines at its sides, by the surface at its bottom and which is open toward space. With negligible fluxes toward space and constant moisture content inside this box, horizontal atmospheric transports (MT) should balance the vertical transports at the surface (PE):

$$\overline{\mathrm{MT}} \cong \overline{\mathrm{PE}} \tag{2}$$

[17] We here focus on the atmospheric moisture budget and its changes and do not draw this further to, e.g., the land's budget, where P-E constitutes the vertical flux which is balanced by river discharge and groundwater flow. In ECHAM5, specific humidity and wind are directly derived from the prognostic variables divergence and vorticity and water vapor whereas P and E are derived diagnostically with several parameterizations and assumptions regarding soil and cloud properties. Specific humidity and winds are available as instantaneous values four times daily at 0, 6, 12, and 18 UTC representative for the 180 s integration time steps whereas P and E are available as 6 hourly accumulated values.

[18] MT across the boundary line is usually given in kg s^{-1} per *m* in the horizontal and per hPa in the vertical to enable comparison of the strength of vertical profiles of MT toward land areas of different sizes. When comparing with PE, however, the unit is transferred to kg m^{-2} yr^{-1}. Respective area sizes and boundary lengths used are listed in Table 1.

[19] We applied the same methodology to ERA-interim [*Simmons et al.*, 2007; *Dee and Uppala*, 2009; *Dee et al.*, 2011] high resolution reanalysis data valid for the period 1989–2008 to compare our model-based results with. Apart from some biases, especially for the smaller islands, the values are very similar to the ECHAM5 derived C20 scenario. For the sake of brevity, and because here we are mainly interested in the change of moisture transport characteristics, we only show the budget derived from ERA-interim in Figure 2.

Table 1. Acronyms, Sizes of Land Areas for Which Moisture Transports Are Calculated and Their Boundary Lengths

Acronym	Name	Area Size (km^2)	Length of Boundary (km)
Continents			
AFR	Africa	29,322,000	33,974.27
ASI	Asia	40,606,300	79,960.32
NAM	North America	23,517,900	58,565.41
SAM	South America	17,831,300	30,792.23
EUR	Europe	9,936,810	27,542.39
AUS	Australia	7,652,370	19,223.94
ANT	Antarctica	13,897,100	27,308.23
Islands			
GRL	Greenland	2,164,010	12,219.97
ICE	Iceland	95,655.9	1696.60
SPZ	Spitsbergen	63,941.4	2429.41
NSM	Novaya Zemlya	77,288.3	2551.43
GBR	Great Britain	3,04,092	5046.83
NZL	New Zealand	264,784	5220.52
IND	Indonesia	2,891,110	42,833.78
CUB	Cuba	1,93,939	5743.46
MAD	Madagascar	5,96,059	4518.45
JAP	Japan	3,45,984	7741.68
Tot	Total	149,761,000	3,67,369

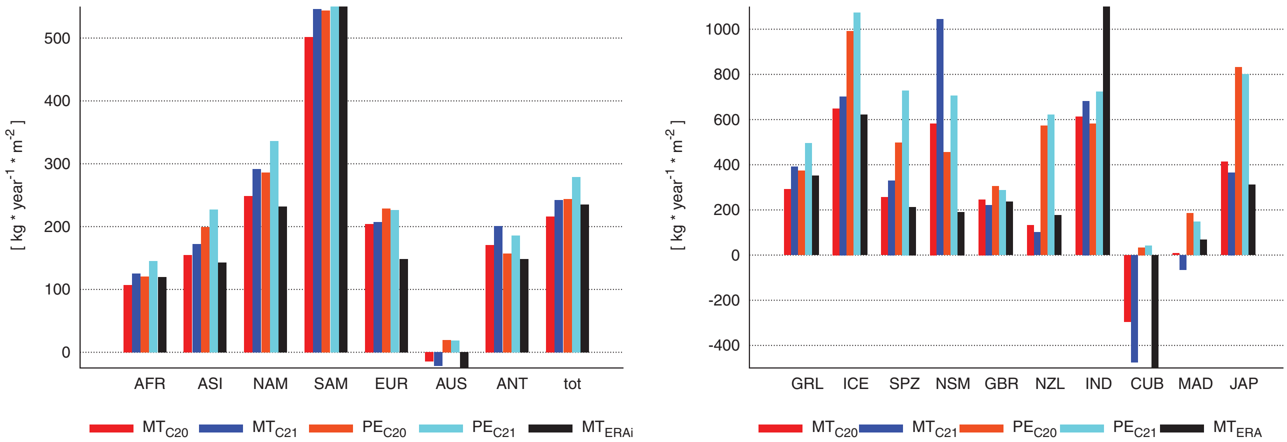

(a) CONTINENTS (b) ISLANDS

Figure 2. Moisture budgets in C20 and C21. Atmospheric moisture budgets over investigated land regions in C20 and C21 derived from transports and precipitation-evaporation. Also shown are the budgets derived from ERA-interim.

3. Results

3.1. General Budgets in C20 and Projected Changes Toward C21

[20] The atmospheric moisture budgets for C20 and for C21 derived from the atmospheric moisture transports (MT) and from the PE balance are shown in Figure 2. Additionally, MT as derived from ERA-interim is shown. Generally, our values are in good agreement with the work by *Trenberth et al*. [2007], who estimated the budgets for the period 1979–2000 from reanalysis data and with the values we calculated from ERA-interim. For the total land mass, we get a C20 budget of $MT_{tot} = 216\ \text{kg} \cdot \text{m}^{-2} \cdot \text{yr}^{-1}$ and $PE_{tot} = 244\ \text{kg} \cdot \text{m}^{-2} \cdot \text{yr}^{-1}$. This is in the same order of magnitude as the values of $\approx$280 kg m^{-2} yr^{-1} which we inferred from *Trenberth et al*. [2007] using our land area data in Table 1 and as those we got from ERA-interim ($\approx$235 kg m^{-2} yr^{-1}). Note that both use a different time period and a different type of data at a different resolution.

[21] Per area unit by far the highest net input of water in the order of 500kg $\cdot$ yr^{-1} $\cdot$ m^{-2} is experienced by South America (SAM), followed by NAM with an input in the order of 300kg $\cdot$ yr^{-1} $\cdot$ m^{-2}. Inputs into Europe (EUR), Asia (ASI) and Africa (AFR) are lower and between 100 and 200kg $\cdot$ yr^{-1} $\cdot$ m^{-2}. The same holds for the *Trenberth et al*. [2007] data and for ERA-interim in which SAM is the wettest continent, too. However, *Trenberth et al*. [2007] present the total amount of water in mass per time, whereas our values are given per area unit (m^{-2}). If we convert their values to our units we get 538kg $\cdot$ m^{-2} $\cdot$ yr^{-1} which again well agrees with our data ($MT_{SAM} = 502\text{kg} \cdot \text{m}^{-2} \cdot \text{yr}^{-1}$, $PE_{SAM} = 544\text{kg} \cdot \text{m}^{-2} \cdot \text{yr}^{-1}$). Please note that all these numbers are summarized for the entire continents and that the spatial distribution of moisture may be highly heterogeneous over each of the continents.

[22] By far the driest continent is Australia (AUS), with small positive numbers for the PE budget, and even negative numbers for MT. By definition in the models prognostic equations, land should not act in the long term as a moisture source for the atmosphere. Thus, the slightly negative budgets of MT_{AUS} may be a concern. However, the PE_{AUS} values are also very low and the absolute difference between MT and PE is not larger than for the other regions. We will discuss plausible reasons for the negative budget associated to sampling issues related to the diurnal cycle of transports later in section 3.3.

[23] A general feature when both ways of estimating the budget are compared is a bias with PE in most cases being higher than MT. However, MT should nearly compensate PE according to the relation in equation (2). This should especially be the case in the model experiments due to reasons of mass conservation. We demonstrate below that these biases are due to the different nature of the two measures compared, based on instantaneous variables at the same four times of the day for MT on the one hand and on the accumulated P and E on the other. We will discuss the details of the origin of these differences later in section 3.3.

[24] Our data are consistent with the expectation of the tropics to become wetter and the subtropics to become drier in response to a warmed atmosphere. AUS and the islands of Japan (JAP) and Madagascar (MAD) which are at least partly situated within the subtropics see a drying from C20 toward C21. In accordance, Indonesia (IND) solely situated within the tropics sees a wettening, while the tropical island of Cuba (CUB) shows a slight wettening at least when PE data are applied.

[25] Despite the bias between both ways of estimating the budget, the sign of change generally is consistent. EUR, CUB, and New Zealand (NZL) are the only areas for which the sign of change is different between budgets of MT and PE. For EUR, this difference is small and we conclude that there is no significant response to warming of the budget for EUR. For CUB and NZL, the differences are large. This at least partly relates to the diurnal sampling as discussed later in section 3.3.

[26] We conclude that apart from some subtropical islands, a higher net amount of moisture is projected to be transported toward the continents in a warmed climate. This change is consistent in the MT and PE budgets of the ECHAM5 model although a bias exists between both ways of estimating the budget. For most of the areas, the change

Table 2. Difference of Mean MT of C21 and C20 and Variance of Yearly Mean MT of C20

Region	$MT_{C21}-MT_{C20}$ (kg y^{-1} m^{-2})	Variance of Yearly Mean MT_{C20} (kg y^{-1} m^{-2})
Continents		
AFR	0.50064	0.711805
ASI	0.27311	0.101538
NAM	0.54714	0.113431
SAM	0.81529	0.629954
EUR	0.03825	0.139178
AUS	−0.091572	0.667951
ANT	0.48989	0.0228815
Islands		
GRL	0.56127	0.0219486
ICE	0.09498	0.0212047
SPZ	0.062093	0.00121847
NSM	0.443353	0.0565046
GBR	−0.047684	0.0201756
NZL	−0.051386	0.0229488
IND	0.14767	0.108532
CUB	−0.192553	0.00769478
MAD	−0.30237	0.272233
JAP	−0.067087	0.0855045
tot	0.32578	0.0185408

of the budget is higher, in many cases much higher, than the variance of the yearly net MT (Table 2). For the total shoreline, the increase of the net MT is more than 15 times its variance. We thus conclude the increase of MT is significant.

3.2. The Vertical Profiles of Moisture Transports

[27] We have previously highlighted how important it is to investigate moisture transports at high spatial and temporal detail, because the vertical profiles are inaccurate in low resolution data. For the convective regions in the tropics, this shortcoming led to an underestimation of the midlevel outward transports of moisture and thus to an overestimation of the total budget [*Zahn and Allan*, 2011]. We here also look at the vertical profiles of transports, averaged along the borderlines of each of the areas in C20 and C21 (Figure 3) and for some of the continents even at very high detail.

[28] For those continents and islands dominated by tropical circulation regimes (SAM, AFR, IND, MAD, and CUB), we find a similar pattern of a strong lower level inward transport, but a strong midlevel outward one exists as well at the same time. The lower level transports exceed the mid and upper level transports and the resulting budgets are positive. The importance of the mid and upper level outward transport becomes evident when SAM and AFR are compared, both approximately covering similar latitudes and receiving most of their moisture from the easterly trades [e.g., *van der Ent et al*. 2010, Figure 1]. Accordingly, the mean lower level inward transports per *m* are very similar in strength. At the upper levels, outward transports are about twice as strong for AFR than they are for SAM, which is largely due to the Andes mountain range stretching from north to south. At their eastern side, orographically induced rain takes moisture out of the atmosphere leaving dry air to be transported outward along large parts of SAM's western coast. Thus, outward moisture transport is generally weak here (supporting information Figures S4j and S4k).

[29] These characteristics of lower level inward and midlevel outward transports which constitute the tropical moisture transport regime can also be found for MAD, IND, and CUB.

[30] Moving pole-ward, we find the subtropical moisture transport regimes over continents which are dominated or strongly influenced by the subtropics, AUS, ASI, and NAM. These areas show a tropical vertical pattern, but intensities of transports are much lower, at low levels as well as at mid and upper levels. Among the three regions, AUS has strongest in and outward transports, whereas the subtropical profiles of NAM and ASI are to a large extent reduced when averaging with the lower values along their extratropical boundaries.

[31] Two of the continents, EUR and Antarctica (ANT), are mostly or entirely located outside the tropics and subtropics. For these two, we find a reversed vertical pattern. They, on average, receive their moisture at the midlevels while losing it at the lower ones. This pattern is confirmed by the profiles of all the extratropical islands. The extratropics receive the majority of moisture when cyclones are moving toward the land driven by the westerly Jet-streams. In such situations, there is a coincidence of higher moisture due to convection and higher wind speeds at midlevels, which may lead to the maximum of moisture input here.

[32] On the right hand-side in Figure 3, the projected changes of MT toward C21 are shown. The strength of MT in C21 is given as a percentage relative to C20 at each level below $\approx$300 hpa. Note that at altitudes at which the profiles turn from positive toward negative, very small numbers or numbers opposite in sign are possible. Here division by very small numbers or division of numbers of different sign may lead to very large or negative percentage numbers.

[33] For all continents apart from EUR and also for all of the islands, we find a strengthening of moisture transports in the order of 30%, with exceptions at few levels only due to the aforementioned reason. This denotes an intensification of the hydrological cycle over all continents in response to warming. In our previous work [*Zahn and Allan*, 2011, 2013] for the convective regions, we found the intensification being caused by increases in the amount of atmospheric moisture, and thus in PWC, which together with the wind vectors determines MT (equation (1)). We find a similar situation for PWC here (Figure 4). Along all regions, PWC has strong maxima at the lower levels. Except some of the northern polar regions (Greenland (GRL), Novaya Zemlya (NSM), and Spitsbergen (SPZ)) increases toward C21 are in the order of $\approx$20% here, and are increasing with altitude to $\approx$40% at about 400 hPa. This vertically growing increase follows theoretical considerations, in which moisture in a warming atmosphere increases following the Clausius-Clapeyron equation. Following this equation, colder air, i.e., air at higher latitudes or altitudes responds to warming with a higher percentage change in specific humidity than does warmer air near to the surface [*Allan*, 2012]. This difference in the relative response of specific humidity highlights how important it is to investigate any changes of MT in detail using the vertical profiles, especially in areas where upper level transports are in the same order of magnitude as at lower levels.

[34] However, such uniform patterns along the boundaries as suggested by these mean vertical profiles are just

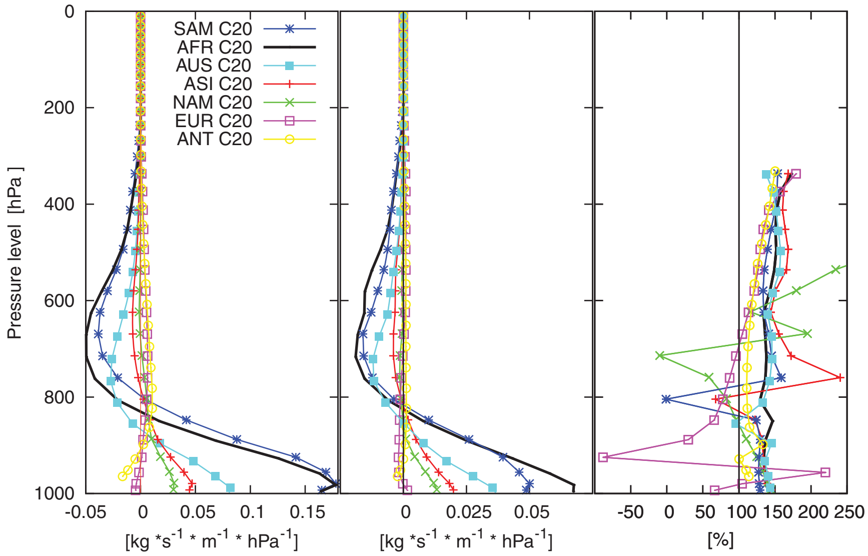

(a) CONTINENTS

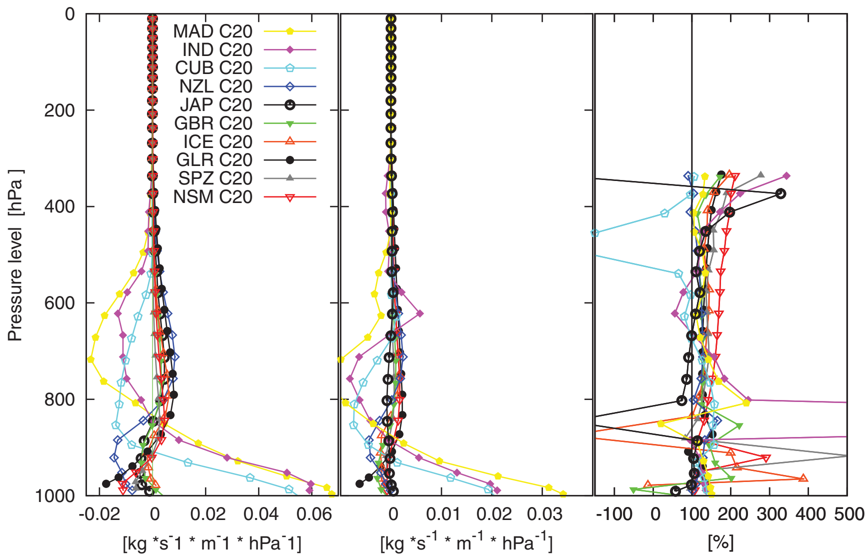

(b) ISLANDS

Figure 3. Vertical profiles of MT in C20 and C21 and percentage change toward C21. (left) Mean vertical profile of moisture transports in C20. (middle) Mean vertical profile of moisture transports in C21. (right) Percentage change C20 toward C21. (top) For the continents. (bottom) For the islands. Note that percentage values can be negative if sign of transport changes. Also note that values can become huge for transports close to zero and thus percentage changes are only given for the low and midlevels in which most of the transports take place. Note the different scales for continents and islands.

valid for the continents as a whole, and they may well locally differ. To illustrate this we have plotted what we call the MT_{wall} for the major continents in Figures 5 and 6 (and also from different perspectives in supporting information Figures S1–S6). The subscript "wall" denotes MT as if transported through an imaginary wall build along the shorelines. These figures show the vertical profiles of MT_{wall} at each location and altitude of the boundaries in C20 and C21 and their difference from four different viewing angles. Note that the boundary lines follow the ECHAM5 model grid and are either in zonal or meridional direction. Thus prevailing winds at 45° angle to the latitudes or longitudes may lead to the alternating blue-red patterns which can be seen, e.g., along the north-west African, northern Australian, or north-east South American coasts.

[35] One of the more complex examples of a vertical profile is found at the west coast of AUS, which has inward MT_{wall} at low levels, outward MT_{wall} at midlevels and inward MT_{wall} again at high levels (supporting information Figures S6j and S6k). The same holds for some parts of the south western African coast. Very uniform patterns are found along the western and eastern coasts of NAM and EUR. In accordance with the prevailing westerlies at these latitudes, inward MT_{wall} is found along almost the entire

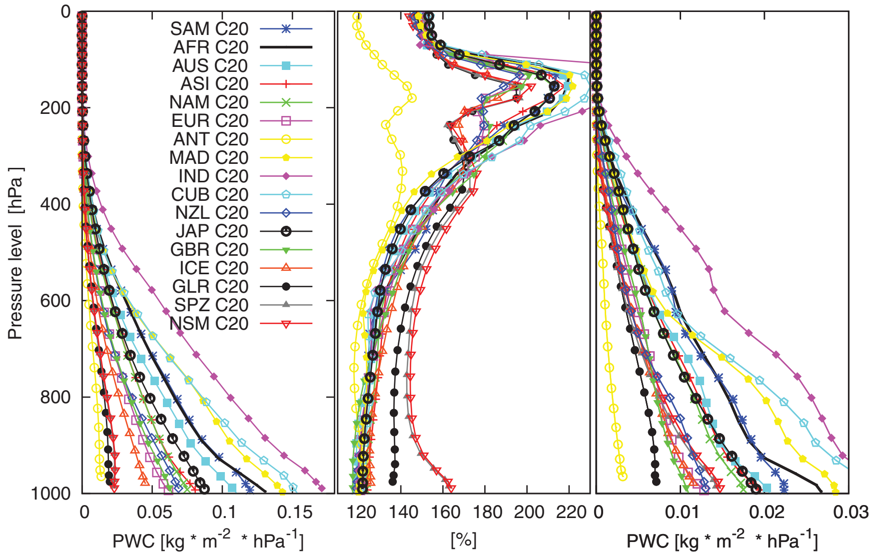

Figure 4. PWC in C20 and change. Mean vertical profile of the precipitable water content per area unit and hPa along the boundaries of our regions in C20 (left), percentage change toward C21 (middle), and absolute change toward C21 (right).

western and outward MT_{wall} along the eastern coasts here. The total lower level inward MT_{NAM} is caused by higher moisture loads in the west than in the east. It should be noted that the eastern boundary of EUR is no coast, but cuts through land separating EUR from ASI. The Southern Hemisphere counterpart of this westerly wind pattern is visible along the southern tip of SAM, where vertically uniform westerlies cause inward transport along its west coast's and outward transport along its east coast's whole vertical.

[36] The pattern of C21 change is shown in the right hand side columns of Figures 5 and 6 (supporting information Figures S1–S6). Generally, there is an intensification of both, inward as well as outward transports, i.e., if over any of the $n_b{\cdot}n_l$ given boundary segments MT_{wall} in C20 is positive/negative it still is in C21, but the respective absolute value is stronger. Such an intensification is seen at more than 80% of the individual boundary segments. This indicates changes of MT_{wall} and thus of continental moisture budgets are dominated by changing intensities of wind/PWC rather than being caused by major shifts of circulation regimes, or in other words: we find an intensification of wettening across already wet boundaries and an intensification of drying across already dry ones.

[37] There are only few exceptions for which this pattern is not true. One is found in EUR along the west coast of Spain. Here in C20 inward MT_{wall} is found, which in C21 weakens strongly (supporting information Figures S5j and S5k) and leads to the red colors in supporting information Figure S5l. This drying is in accordance with a shift in the North Atlantic storm track, which is projected to move northward with climate warming [*Bengtsson et al.*, 2006]. Storm systems carry large amounts of moisture and are a major contributor to the moisture budgets in EUR. Fewer storms touching Spain thus reduce the amount of water entering the continent here. Similarly, signs of a reversed pattern at the south western coast of SAM (supporting information Figures S4i and S4l) and at the northern Mexican coast of NAM may also be linked to a pole-ward shift of the western Pacific storm tracks in both hemispheres.

[38] Some further regions exhibiting such a reversed pattern are the southern tip of India and Sri Lanka and the northern coast of Russia in ASI. The first is probably linked to a shift in the latitude of the easterly trade winds in the Indian Ocean in C21. The latter presumably is linked to more moist Arctic air in C21, when more frequent ice free ocean conditions give rise to more frequent evaporation, and warmer air can carry more moisture. If under these C21 conditions, the wind is directed toward land in rare occasions MT_{wall} may be much higher resulting in a weaker overall inward transport.

[39] We conclude that we find different vertical MT profiles indicative for regions of the extratropics, subtropics, and tropics, with the subtropical profile being a transition between the two others. MT toward land generally intensifies meaning that boundary segments of inward MT show a stronger inward MT in C21 and boundary segments with outward MT a stronger outward one. There are only few exceptions from this rule.

3.3. Explaining Differences Between MT and PE With the Diurnal Cycles

[40] In section 3.1, we referred to two concerns in our results, negative moisture budgets for two of the land regions, AUS and CUB, and to a systematic bias between the two ways of estimating the budget, via MT and PE. One can blame numerical issues for these differences, but we here give a more plausible explanation related to the properties of the diurnal cycle. The diurnal cycle is captured in the accumulated P and E values, but perhaps not in the four-times daily MT values.

[41] Precipitation in a certain area is known to have a distinct diurnal cycle. It is shown in *Lee et al.* [2007] that over the ocean maxima in P are usually found during the early morning hours after humidity rises in response to radiative warming and evaporation after dawn. Over land,

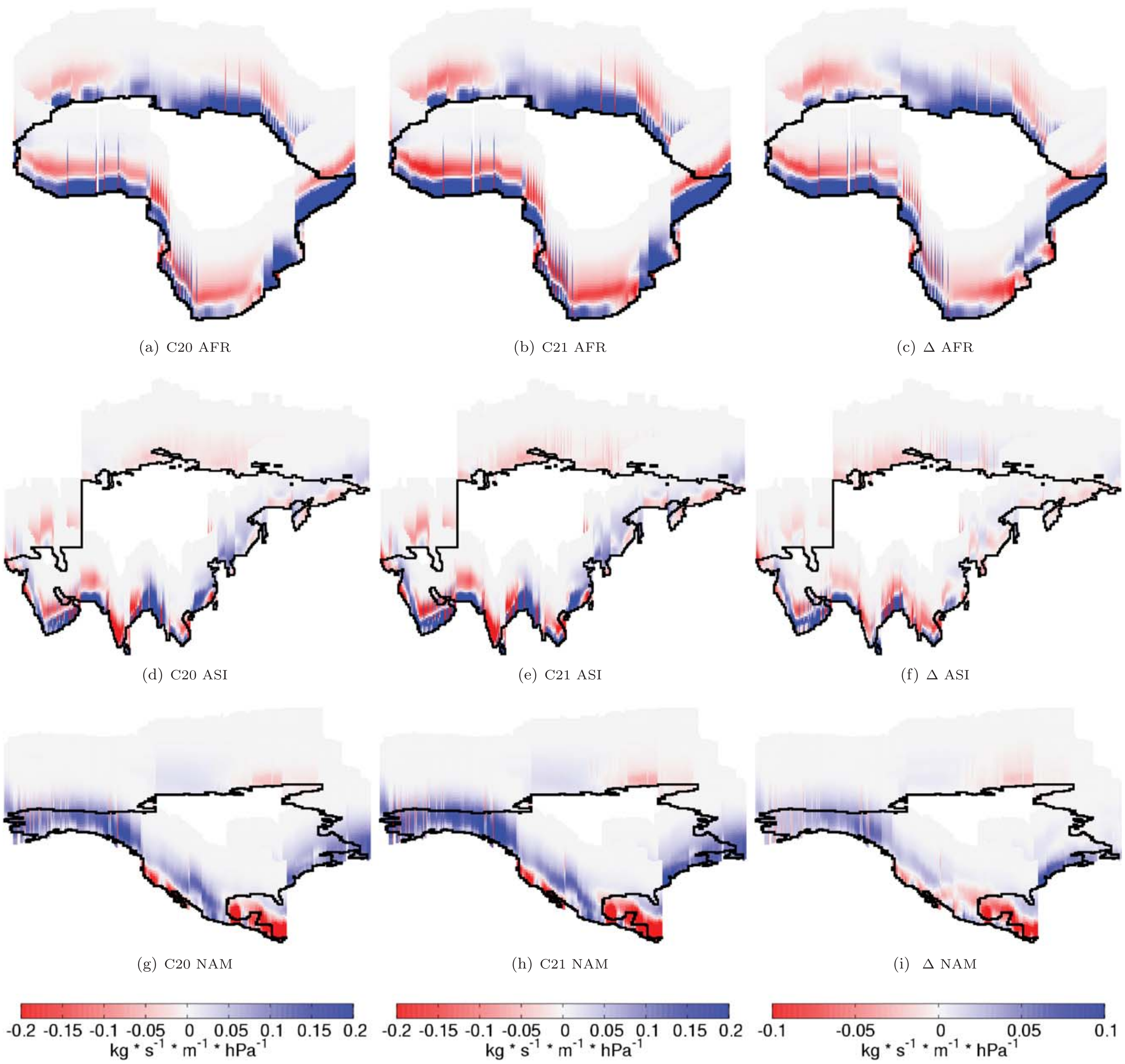

Figure 5. MT_{wall} for AFR, ASI, and NAM. MT wall for AFR, ASI, and NAM viewed from the south. For other perspectives of the same figure, please see the supporting information. (left) C20, (middle) C21, and (right) C21-C20.

however, maximum P is normally found at the later afternoon/early evening after moist air from over the ocean has been shifted into a certain area. Locally, these times of maximum P may differ, but it was shown in *Dai et al*. [2007] that for AUS, at least in summer and in its south eastern area, P has its maximum between 3 and 6 P.M. local time, exceeding P at all the other times more than twice. We do not know of any such study for E or moisture transports and their dependence on the diurnal cycle but assume it is similarly strong as for P.

[42] Our vertical MT profiles for AUS are available at sampling times 0, 6, 12, and 18 UTC corresponding to local times around 9, 15, 21, and 3 O'clock. We break down MT at these times in Figure 7. The four graphs clearly show two different regimes. The local time 15 and 21 O'clock graphs show a distinct inward MT_{AUS} at lower levels and outward MT_{AUS} at higher ones, while at 3 and 9 O'clock outward MT_{AUS} is found almost over the whole vertical. Thus, there is a strong diurnal cycle of MT_{AUS} and the net transport can either be negative or positive depending on the time of the day. This implies a high sensitivity of the total time mean moisture budget to maxima of the transport. However, if we assume a daily maximum of MT for AUS around 18 O'clock local time, this maximum occurs just between two sampling times of our model data. Accordingly, total inward MT_{AUS} is systematically too low. If at the same time the outward MT is covered more realistically, because no such distinct maxima at particular times exist, the total MT budgets will be underestimated as a result as well. In the case of AUS (and of CUB), this

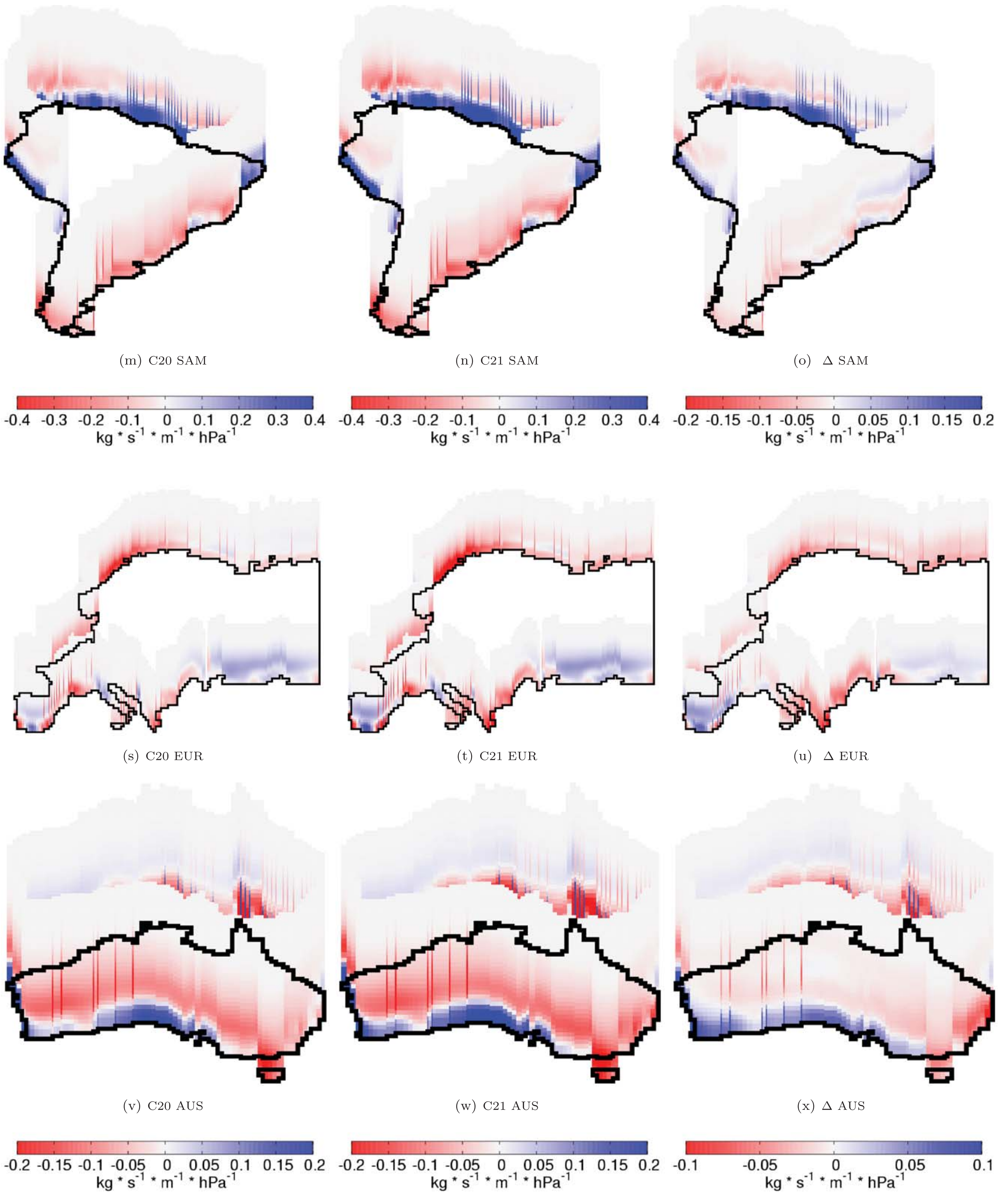

Figure 6. MT_{wall} for SAM, EUR, and AUS. MT wall for SAM, EUR, and AUS viewed from the south. For other perspectives of the same figure, please see the supporting information. (left) C20, (middle) C21, and (right) C21-C20.

underestimation even results in a negative value for the otherwise close to zero total MT-budget.

[43] A similar time-of-the-day dependence is found for almost all of the other regions as well (Figure 8 and supporting information Figures S7–S10) and is stronger the stronger the local day-night differences in a region are. We believe this is the reason for the biases between MT and PE in Figure 2. This may also explain why the bias is lower for

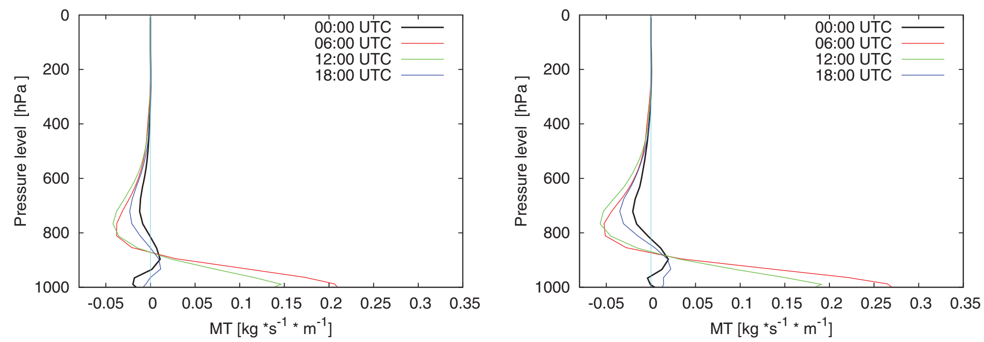

(a) AUS C20 (b) AUS C21

Figure 7. MT in AUS at sampling times. The mean vertical profile of MT across the boundary of AUS at 0, 6, 12, and 18 UTC, respectively. Note that local time in AUS is between UTC+8 and UTC+10.

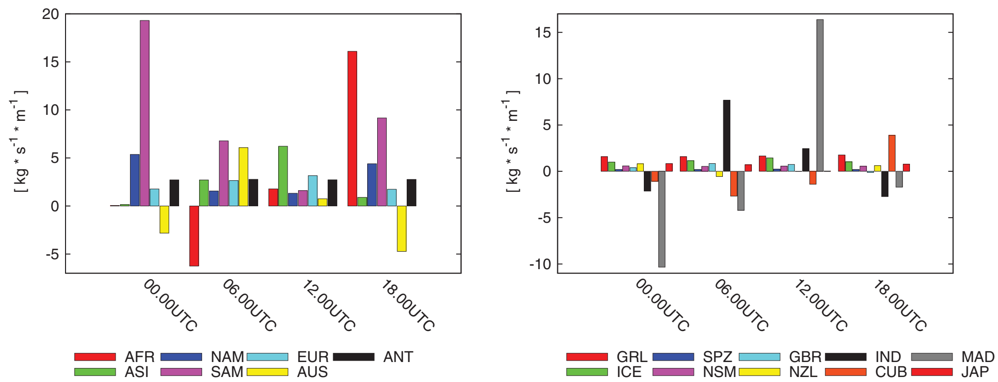

(a) CONTINENTS (b) ISLANDS

Figure 8. Diurnal cycle of moisture transports. Instantaneous MT representative for the 180 s integration time steps at 0, 6, 12, and 18 UTC for (a) the continents and (b) for the islands.

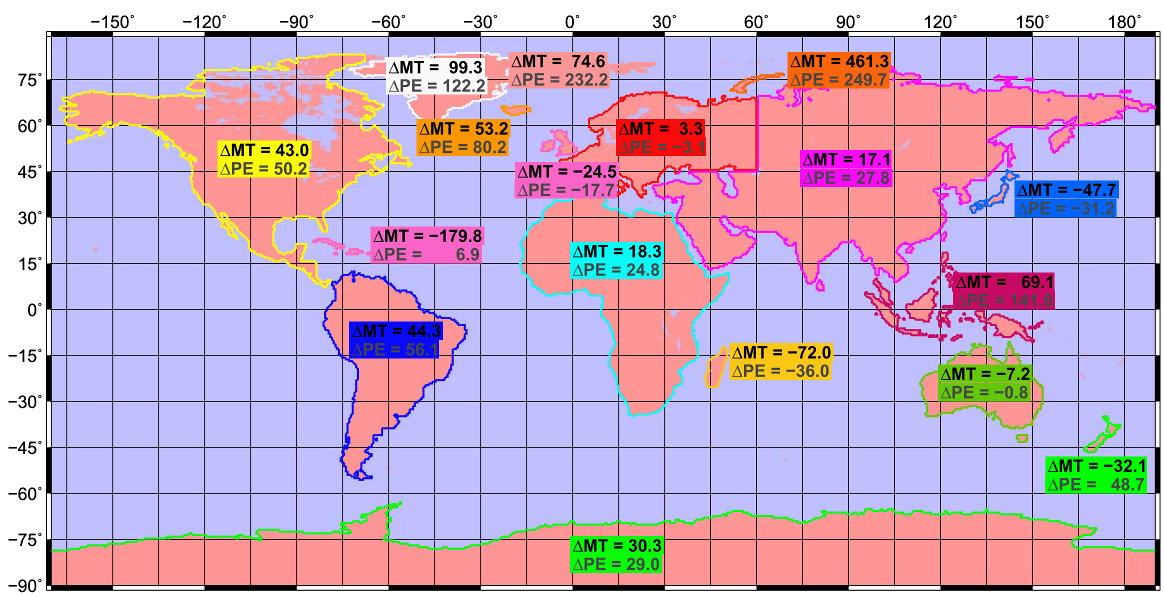

Figure 9. Summary of changes in the moisture budget. The difference of the moisture budget of each continent and island from MT and PE. Δ denotes difference of C21 minus C20 values. Unit is kg yr^{-1} m^{-2}.

ANT and EUR where the diurnal cycle is weak, but stronger for the other regions.

[44] A bias due to temporal sampling has been reported in *Ropelewski and Yarosh* [1998] and has been further investigated in *Yarosh et al*. [1999]. They calculate the water budget for a North American area once based on 3 hourly and on 12 hourly model output and find spatial and temporal sampling dominating the influence on the bias. With regards to temporal sampling, our study extends these finding from a North American area to a global perspective.

[45] Along a long boundary which extends over various time zones, this effect may be compensated, because it is more likely that the maximum inflow is captured at least at some place. On the other hand, the MT budget can hardly reach the actual values, because it is almost certain that maximum MT is not captured at many places. These two points may be the reason why the bias of MT is systematically lower over the continents, but the difference is moderately large.

[46] Including the maximum MT is less likely for a small boundary as those around the various islands and there is only a minor compensating effect. Accordingly, biases here can become much more pronounced (Figure 2b). In the case of IND, however, the maximum seems to be captured quite well and IND is the only tropical region with similar MT and PE.

4. Summary

[47] We have calculated landward moisture transports globally across the shorelines with high space and time resolution model data from one realization of a 20th and one realization of an anthropogenically warmed 21st century. In line with previous studies, we found higher in- and outward transports and thus an intensification of the hydrological cycle. For all tropical and subtropical regions, these changes result in a higher budget. Hence, more water may be expected to be available in future in total.

[48] We also found that the inflow of moisture will intensify at places where we have an inflow today. At boundaries at which the transport is directed seaward today, this drying will become stronger in our simulated future. This means that the additional water enters Africa (or other continents) where already wet conditions prevail today, and at already dry places the availability of water decreases further potentially worsening the food supply situation here. The changes of the budget are summarized for all regions in Figure 9.

[49] We found a strong diurnal cycle of the landward moisture transports. We suggest that the four-times daily instantaneous values do not capture the maximum moisture transport transports. This explains a systematic bias when the resulting budget is compared to the one from precipitation-evaporation, which is based on the accumulated values collected over the whole course of a day.

[50] **Acknowledgments.** The simulations were performed with the ECHAM5 model developed at the Max-Planck Institute for Meteorology, Germany, at HLRN (Norddeutscher Verbund für Hoch und Höchstleistungsrechnen). We are thankful to Noel Keenlyside and Kevin Hodges for help with these data and for discussions. M. Z. was funded by the NERC PREPARE project, NE/G015708/1.

References

Allan, R. P. (2012), The role of water vapour in Earth's energy flows, *Surv. Geophys.*, *33*, 1–8, doi:10.1007/s10712-011-9157-8.

Bengtsson, L., K. I. Hodges, and E. Roeckner (2006), Storm tracks and climate change, *J. Clim.*, *19*, 3518–3543, doi:10.1175/JCLI3815.1.

Carvalho, L. M. V., A. E. Silva, C. Jones, B. Liebmann, P. L. S. Dias, and H. R. Rocha (2011), Moisture transport and intraseasonal variability in the South America monsoon system, *Clim. Dyn.*, *36*(9–10), 1865–1880, doi:10.1007/s00382-010-0806-2.

Dai, A., X. Lin, and K.-L. Hsu (2007), The frequency, intensity, and diurnal cycle of precipitation in surface and satellite observations over low- and mid-latitudes, *Clim. Dyn.*, *29*, 727–744, doi:10.1007/s00382-007-0260-y.

Dee, D. P., and S. Uppala (2009), Variational bias correction of satellite radiance data in the era-interim reanalysis, *Q. J. R. Meteorol. Soc.*, *135*, 1830–1841, doi:10.1002/qj.493.

Dee, D. P., et al. (2011), The era-interim reanalysis: Configuration and performance of the data assimilation system, *Q. J. R. Meteorol. Soc.*, *137*(656), 553–597, doi:10.1002/qj.828.

Drumond, A., R. Nieto, L. Gimeno, and T. Ambrizzi (2008), A Lagrangian identification of major sources of moisture over Central Brazil and La Plata Basin, *J. Geophys. Res.*, *113*, D14128, doi:10.1029/2007JD009547.

Durán-Quesada, A. M., L. Gimeno, J. A. Amador, and R. Nieto (2010), Moisture sources for central America: Identification of moisture sources using a Lagrangian analysis technique, *J. Geophys. Res.*, *115*, D05103, doi:10.1029/2009JD012455.

Gimeno, L., A. Drumond, R. Nieto, R. M. Trigo, and A. Stohl (2010a), On the origin of continental precipitation, *Geophys. Res. Lett.*, *37*, L13804, doi:10.1029/2010GL043712.

Gimeno, L., R. Nieto, R. M. Trigo, S. M. Vicente-Serrano, and J. I. López-Moreno (2010b), Where does the Iberian Peninsula moisture come from? An answer based on a Lagrangian Approach., *J. Hydrometeorol.*, *11*, 421–436, doi:10.1175/2009JHM1182.1.

Gimeno, L., A. Stohl, R. M. Trigo, F. Dominguez, K. Yoshimura, L. Yu, A. Drumond, A. M. Durn-Quesada, and R. Nieto (2012), Oceanic and terrestrial sources of continental precipitation, *Rev. Geophys.*, *50*, RG4003, doi:10.1029/2012RG000389.

Hagos, S., and L. R. Leung (2012), On the relationship between uncertainties in tropical divergence and the hydrological cycle in global models, *J. Clim.*, *25*, 381–391, doi:10.1175/JCLI-D-11-00058.1.

Held, I. M., and B. J. Soden (2006), Robust responses of the hydrological cycle to global warming, *J. Clim.*, *19*, 5686–5699.

Koster, R., J. Jouzel, R. Suozzo, G. Russell, W. Broecker, D. Rind, and P. Eagleson (1986), Global sources of local precipitation as determined by the Nasa/Giss GCM, *Geophys. Res. Lett.*, *13*(2), 121–124, doi:10.1029/GL013i002p00121.

Lavers, D. A., R. P. Allan, E. F. Wood, G. Villarini, D. J. Brayshaw, and A. J. Wade (2011), Winter floods in Britain are connected to atmospheric rivers, *Geophys. Res. Lett.*, *38*, L23803, doi:10.1029/2011GL049783.

Lee, M.-I., S. D. Schubert, M. J. Suarez, T. L. Bell, and K.-M. Kim (2007), Diurnal cycle of precipitation in the NASA seasonal to interannual prediction project atmospheric general circulation model, *J. Geophys. Res.*, *112*, D16111, doi:10.1029/2006JD008346.

Mutua, F., L. Wang, A. Yamamoto, T. Nemoto, M. Kitsuregawa, and T. Koike (2012), Regional climate change and its impacts on future discharges and flow characteristics of the Nyando basin, Kenya, *Ann. J. Hydraul. Eng., JSCE*, *56*, 1–6.

Nakicenovic, N., and R. Swart (Eds.) (2000), *IPCC Special Report on Emissions Scenarios*, Cambridge Univ. Press, Cambridge, U. K.

Nieto, R., L. Gimeno, and R. Trigo (2006), A Lagrangian identification of major sources of Sahel moisture, *Geophys. Res. Lett.*, *33*, L18707, doi:10.1029/2006GL027232.

Numaguti, A. (1999), Origin and recycling processes of precipitating water over the Eurasian continent: Experiments using an atmospheric general circulation model, *J. Geophys. Res.*, *104*(D2), 1957–1972, doi:10.1029/1998JD200026.

O'Gorman, P. A., and C. J. Muller (2010), How closely do changes in surface and column water vapor follow Clausius Clapeyron scaling in climate change simulations?, *Environ. Res. Lett.*, *5*(025207), doi:10.1088/1748-9326/5/2/025207.

Ordóñez, P., P. Ribera, D. Gallego, and C. Peña Ortiz (2012), Major moisture sources for Western and Southern India and their role on synoptic-scale rainfall events, *Hydrol. Processes*, doi:10.1002/hyp.8455.

Quante, M., and V. Matthias (2006), Water in the earth's atmosphere, *J. Phys. IV France*, *139*, 37–61.

Rasmusson, E. M. (1971), A study of the hydrology of eastern North America using atmospheric vapor flux data, *Mon. Weather Rev.*, *99*, 119–135, doi:10.1175/1520-0493(1971)099¡0119:ASOTHO¿2.3.CO;2.

Roeckner, E., et al. (2003), The atmospheric general circulation model ECHAM5. Part I: Model description, *Max Planck Institute for Meteorology Rep. 349*, 127 pp. [Available at http://www.mpimet.mpg.de/fileadmin/publikationen/Reports/max_scirep_349.pdf.]

Ropelewski, C. F., and E. S. Yarosh (1998), The observed mean annual cycle of moisture budgets over the Central United States (1973–1992), *J. Clim.*, *11*, 2180–2190.

Seager, R., N. Naik, and G. A. Vecchi (2010), Thermodynamic and dynamic mechanisms for large-scale changes in the hydrological cycle in response to global warming, *J. Clim.*, *23*(17), 4651–4668, doi:10.1175/2010JCLI3655.1.

Simmons, A., S. Uppala, D. Dee, and S. Kobayashi (2007), ERA-Interim: New ECMWF reanalysis products from 1989 onwards, Newsl. 110, European Centre for Medium-Range Weather Forecasts, Reading, U. K.

Stohl, A., and P. James (2004), A Lagrangian analysis of the atmospheric branch of the global water cycle. Part I: Method description, validation, and demonstration for the August 2002 flooding in central Europe, *J. Hydrometeorol.*, *5*, 656–678, doi:10.1175/1525-7541(2004)005¡0656:ALAOTA¿2.0.CO;2.

Stohl, A., and P. James (2005), A Lagrangian analysis of the atmospheric branch of the global water cycle. Part II: Moisture transports between earths ocean basins and river catchments, *J. Hydrometeorol*, *6*, 961–984, doi:10.1175/JHM470.1.

Trenberth, K. E., A. Dai, R. M. Rasmussen, and D. B. Parsons (2003), The changing character of precipitation, *Bull. Am. Met. Soc.*, *84*, 1205–1217.

Trenberth, K. E., L. Smith, T. Qian, A. Dai, and J. Fasullo (2007), Estimates of the global water budget and its annual cycle using observational and model data, *J. Hydrometeorol*, *8*, 758–769, doi:10.1175/JHM600.1.

van der Ent, R. J., H. H. G. Savenije, B. Schaefli, and S. C. Steele-Dunne (2010), Origin and fate of atmospheric moisture over continents, *Water Resour. Res.*, *46*, W09525, doi:10.1029/2010WR009127.

Viste, E., and A. Sorteberg (2011), Moisture transport into the Ethiopian highlands, *Int. J. Climatol.*, *33*, 249–263, doi:10.1002/joc.3409.

Wentz, F. J., and M. Schabel (2000), Precise climate monitoring using complementary satellite data sets, *Nature*, *403*, 414–416, doi:10.1038/35000184.

Yarosh, E. S., C. F. Ropelewski, and E. H. Berbery (1999), Biases of the observed atmospheric water budgets over the central United States, *J. Geophys. Res.*, *104*(D16), 19,349–19,360.

Zahn, M., and R. P. Allan (2011), Changes in water vapor transports of the ascending branch of the tropical circulation, *J. Geophys. Res.*, *116*, D18111, doi:10.1029/2011JD016206.

Zahn, M., and R. P. Allan (2013), Climate warming-related strengthening of the tropical hydrological cycle, *J. Clim.*, *26*, 562–574, doi:10.1175/JCLI-D-12–00222.1.